Stabilization of a thermoacoustically unstable sequential combustor using non-equilibrium plasma: Large eddy simulation and experiments

Quentin Malé, Shcherbanev Sergey, Impagnatiello Matteo, Noiray Nicolas

Stabilization of a thermoacoustically unstable sequential combustor using non-equilibrium plasma: Large eddy simulation and experiments

Quentin Malé*, Sergey Shcherbanev, Matteo Impagnatiello, Nicolas Noiray*

CAPS Laboratory, Department of Mechanical and Process Engineering, ETH Zürich, Zürich 8092, Switzerland

Abstract

Plasma-assisted combustion using Nanosecond Repetitively Pulsed Discharges (NRPDs) is an emerging technology that enhances the reactivity of fuel-air mixtures, offering significant improvements in operational and fuel flexibility—two crucial features for future sustainable gas turbines. The mechanisms that enable the stabilization of thermoacoustically unstable burners, however, remain unclear. Thus, to investigate the physical phenomena involved, we performed a massively parallel Large Eddy Simulation (LES) of the stabilization of a thermoacoustically unstable sequential combustor by NRPDs at atmospheric pressure. LES is combined with an accurate description of the combustion chemistry and a state-of-the-art phenomenological model for the non-equilibrium plasma effects. In this work, we have validated the simulation framework by comparison with experimental data including acoustic pressure and Heat Release Rate (HRR) signals in both stages of the sequential combustor, and OH-planar laser-induced fluorescence images in the second stage combustion chamber. Hence, this study provides a robust LES framework to study the effects of NRPDs on Thermoacoustic Instabilities (TIs). In addition, the analysis of the LES data reveals a significant decrease of the acoustic energy production in the sequential combustor thanks to the NRPDs. Surprisingly, the steady NRPD actuation generates HRR fluctuations upstream of the combustion chamber, which are in phase opposition to the acoustic pressure, inducing locally a sink term in the acoustic energy balance equation. Moreover, an analysis of the acoustic energy production during the onset of the TI reveals the predominant role of the second stage in developing and sustaining the self-excited TI. The effect of plasma is therefore very effective in stabilizing the system by reducing the acoustic energy production in the sequential stage.

Keywords: Plasma assisted combustion; Thermoacoustic instability; Large eddy simulation; Turbulent combustion; Multiphysics computation

*Corresponding authors.
E-mail addresses:
qumale@ethz.ch (Q. Malé),
noirayn@ethz.ch (N. Noiray).

Information for Colloquium Chairs and Cochairs, Editors, and Reviewers

1) Novelty and Significance Statement

LES of the suppression of a Thermoacoustic Instability (TI) inside a sequential combustor using NRPDs is successfully performed for the first time. The simulation framework is validated by comparison with experimental data including pressure and Heat Release Rate (HRR) signals in both stages, and OH-PLIF in the sequential stage. LES data unravel a damping of the acoustic energy production due to NRPDs. NRPDs generate HRR fluctuations in phase opposition to pressure fluctuations, inducing a sink term in the acoustic energy balance equation. Furthermore, an analysis of the acoustic energy production in both stages shows that the second stage plays a predominant role in the development and sustaining of the self-excited TI. All the aforementioned research outputs bring relevant knowledge for the community to successfully implement NRPD in real systems. NRPD can improve operational and fuel flexibility, crucial features for future sustainable combustion systems.

2) Author Contributions

- Q.M.: Performed the experiments and simulations, developed the numerical methods for plasma assisted combustion, performed the analysis and post-processed the results, discussed the results, wrote the paper.
- S.S: Led and performed the experiments, post-processed the experimental data, discussed the results, reviewed and edited the paper.
- M.I.: Discussed the results, reviewed and edited the paper.
- N.N.: Conceptualized the research idea, designed the combustor, discussed the results, reviewed and edited the paper.

3) Authors' Preference and Justification for Mode of Presentation at the Symposium

The authors prefer **OPP** presentation at the Symposium, for the following reasons:

- PAC can improve turbine operational flexibility, needed for effective wind and solar sources intermittency compensation.
- PAC can be used to burn sustainable fuels of non-conventional composition expected to be produced in the future.
- This work builds up on previous symposium papers/presentations (see Q. Malé, Y. Bechane, D. Lacoste).
- Thermoacoustic instabilities are a well-known problem that needs no extensive introduction.
- This work will provide an opportunity to discuss possible NRPD implementations on existing combustors.

1. Introduction

Combustion systems globally play a dominant role in electric power generation and transportation. Yet, they are the cause of climate change because of their associated CO_2 emissions. Disruptive technologies enabling clean and decarbonized combustion processes are therefore essential for establishing sustainable energy networks. Plasma Assisted Combustion (PAC) is an emerging technology that can play a key role in the development of cleaner and more efficient energy systems [1]. Indeed, Non Equilibrium Plasmas (NEPs) that can be obtained by Nanosecond Repetitively Pulsed Discharges (NRPDs) have been shown to improve ignition and flame stability [2–7] and thus enhance fuel flexibility, which will become more and more important in the future. Moreover, controlling Thermoacoustic Instabilities (TIs) is of major interest to enable lean premixed combustion of sustainable fuels at very low pollutant emission levels.

Research work on the suppression of TIs by NEP is still limited, but promising. The work of Lacoste et al. [2] showed that NRPDs significantly change the response of a lean premixed swirl flame to acoustic perturbations. The authors also investigated a configuration where the flame features a self-sustained TI. NRPDs have been shown to effectively mitigate this instability. Later, the capability of NRPDs to mitigate the response of a lean premixed swirl flame to acoustic excitations has been demonstrated at pressures up to 3 bar [6]. The plasma induces a change in the phase of the Heat Release Rate (HRR) fluctuations in the lower part of the flame. These fluctuations are then in phase opposition to the fluctuations in the upper part of the flame. This mechanism has been identified as potentially responsible for the attenuation of the flame response to excitation. In addition, the capability of NRPDs to mitigate the TI of a wall-stabilized laminar flame was investigated in Ref. [5]. Recently, it has been shown that NRPDs can be used in a turbulent sequential combustor to control TIs with ultra-low plasma power [7]. Also, under certain conditions, the plasma was found to induce a TI involving another acoustic mode.

Explaining how the plasma controls TIs remains an open question that requires in-depth investigation. Addressing this issue is crucial for designing effective systems for real combustors that operate across a wide range of conditions. Understanding the underlying mechanisms can only be done with the help of accurate simulation tools that enable the description of the aerothermochemical state at any point in time and space in complex, realistic, combustors. Some numerical studies of PAC have demonstrated the feasibility of such simulations to study the extension of the lean flame blow-off/stability limit [8–10], the enhancement of ignition [11], and even the formation of pollutants due to NEP [12]. However, the control of TIs by NRPDs has never been studied using numerical simulations. The aim of this work is to fill this gap by performing a joint experimental and numerical study on the control of a thermoacoustically instable atmospheric pressure sequential combustor using NRPDs. To achieve this goal, we have first performed experimental tests using a sequential combustor with adjustable acoustic boundary conditions. Then, we have used massively parallel Large Eddy Simulation (LES) of the full domain to retrieve the self-excited TI observed in the experiments. Subsequently, stabilization by plasma has been simulated using state-of-the-art modeling of the NEP effects [13].

This paper reports the joint experimental and numerical study of the plasma control of the TI, together with the simulation framework that has been successfully set up for this purpose. First, the experimental configuration is presented (Section 2). Then, the simulation methods are described (Section 3). Finally, the experimental and numerical results are discussed (Section 4). The LES data are analyzed to explain the damping of the TI, and to describe the TI that settles in the sequential combustor.

2. Experimental setup

The experiments are performed using a laboratory scale sequential combustor operated at atmospheric pressure (Fig. 1). The first stage consists of an array of 4×4 premixed jet flames. The sequential stage features a dilution air mixer with large lateral vortex generators and multiple air injection holes for rapid mixing, a Sequential Burner (SB) in which fuel is injected axially and mixes with the co-flow of hot vitiated air, a pin-to-pin electrodes arrangement in the SB which enables NRPD generation upstream of the SB outlet, and the second stage Combustion Chamber (CC). The test rig features an adjustable acoustic outlet boundary condition based on the control of the outlet cross-sectional area during operation, using a conical piston. Varying this area changes the acoustic reflection coefficient. The piston position is set so that the sequential combustor is thermoacoustically unstable before NRPDs are applied.

Throughout this study, the first stage is fed with 17.7 g/s of premixed CH_4-air mixture at an equivalence ratio of 0.7 and a temperature of 518 K. After combustion, the hot products are diluted with 18 g/s of air at ambient temperature. A CH_4-H_2 fuel blend is used in the sequential stage. The mass flows of methane and hydrogen are 0.6 g/s and 0.07 g/s, respectively. The global equivalence ratio in the second stage is 0.55. The thermal power of the first stage is 35 kW, and of the second stage 38.4 kW. High voltage pulses are applied at a pulse repetition frequency of 10 kHz to locally generate multiple NRPDs between the electrodes. The applied voltage is 9 kV, resulting in a mean deposited energy $E^p = 3.56$ mJ. More details on the discharge characteristics are given in the supplementary materials. Two different cases are investigated: "NRPD OFF" where the combustor is thermoacoustically unstable with a predominant TI at 308 Hz and "NRPD ON" where the combustor is sta-

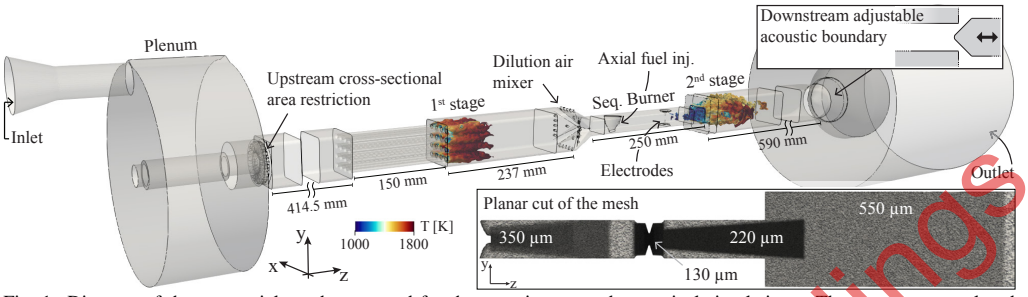

Fig. 1: Diagram of the sequential combustor used for the experiments and numerical simulations. The temperature colored iso-surfaces of HRR depict the two flames. The inset on the bottom right shows a view of the mesh in the sequential stage with the characteristic cell size annotated.

bilized by the NRPDs (Fig. 2).

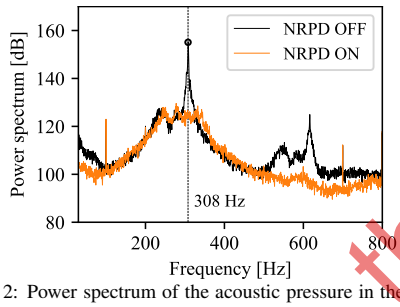

Fig. 2: Power spectrum of the acoustic pressure in the first stage CC normalized with a reference pressure of 20 μPa, with and without NRPD. The amplitude peak at 308 Hz is successfully suppressed by the NRPDs.

Each stage of the sequential combustor is equipped with a photomultiplier and a piezoelectric sensor to record fluctuations in pressure P' and an indication of the volume-averaged heat release Q'. The first and second piezoelectric sensors are located 86.5 mm downstream of the first burner outlet and 370.4 mm downstream of the SB outlet, respectively. In addition, high-speed cameras are used to visualize the spatial distribution of the OH^* chemiluminescence, with a frame rate of 2 kHz. Due to the significantly higher intensity of plasma-induced OH^* chemiluminescence compared to flame chemiluminescence, an optical barrier is used to mask the location of the discharge and avoid potential damage to the equipment. OH-Planar Laser-Induced Fluorescence (PLIF) is used in the second stage CC to visualize the effects of the plasma on the flame. The laser sheet is generated in the x-z plane, while the ICCD camera is oriented in the y-direction. PLIF images are acquired at a sampling rate of 10 Hz and are corrected for the intensity distribution along the laser sheet. More details on the experimental setup including optical diagnostics are given in the supplementary materials.

3. Numerical model and methods

3.1. Plasma modeling

Solving the electric field, the electron energy, the continuity equations for charged and excited species, in addition to the Navier-Stokes equations for reactive flows is very challenging and requires very high computational resources [14–16]. Still, the integration of NEP effects in three-dimensional simulations of turbulent reactive flows inside complex geometries can be achieved with simplified models that incorporate the primary plasma effects for the considered study. In this work, the phenomenological model recently developed by Barléon et al. [13] is used. As in Ref. [17], the discharge power $\dot{E}^p$ is divided into three contributions:

$$\dot{E}^p = (\alpha_{\text{chem}} + \alpha_{\text{heat}} + \alpha_{\text{vib}})\,\dot{E}^p\,, \qquad (1)$$

where α_{chem}, α_{heat} and α_{vib} are the discharge energy fractions that go into chemical effects, fast gas heating and vibrational excitation, respectively. The chemical energy fraction is divided into $P = 5$ global processes $\alpha_{\text{chem}} = \sum_{j=1}^{P} \alpha_j$ taking into account the dissociation of O_2, CH_4, H_2O and CO_2. The discharge energy fraction coefficients α characterize the discharge effects. They are computed from an analysis of the species production rate from plasma processes issuing from detailed plasma-combustion kinetics calculations [13, 18]. More details on the processes considered and on the determination of the coefficients are given in the supplementary materials. For the discharge characteristics that are considered in this work, the energy fractions are estimated as $\alpha_{\text{chem}} = 0.358$, $\alpha_{\text{heat}} = 0.346$ and $\alpha_{\text{vib}} = 0.296$. The main chemical process involved is the dissociation of O_2 by direct electron impact or dissociative quenching of electronically excited N_2. The discharge energy fraction going into this process is estimated to be 0.184.

This modeling approach has been successfully applied in a LES framework to study turbulent flame ignition [11], turbulent combustion enhancement [8], lean stability limit extension [9, 10] and even NO_x formation [12].

3.2. Large eddy simulation

LES is performed using the AVBP [19, 20] unstructured cell-vertex massively parallel code solving the compressible multi-species Navier-Stokes equations. A third order accurate Taylor–Galerkin scheme is adopted for discretization of the convective terms [21]. The effects of the unresolved small-scale fluid motion are modeled using the SIGMA subgrid-scale model [22]. Navier-Stokes Characteristic Boundary Conditions (NSCBCs) [23] are imposed at the inlets and at the outlet. The main inlet and the outlet are located far enough so that non-reflective boundary conditions can be realistically set. The acoustic boundaries of the sequential combustor are imposed by the geometry of the upstream and downstream cross-sectional area restrictions (Fig. 1). Boundary layers are handled with a law-of-the-wall formulation [24]. Walls are modeled as isothermal with a temperature of 600 and 400 K for the air-cooled quartz windows and water-cooled aluminium parts, respectively. The quartz parts are the side walls of the SB and the CCs, designed for optical access. Description of the chemical kinetics relies on Analytically Reduced Chemistry (ARC) to accurately describe autoignition, plasma-enhanced reactivity, flame consumption rate and stretch response. The ARC mechanism has been specially constructed for the conditions of the sequential combustor including PAC [9], starting from the CRECK mechanism [25]. The final ARC mechanism contains 23 species (7 of them in quasi-steady state) and 154 reactions (see supplementary materials of Ref. [9]). The mixture transport properties are modeled using a constant Prandtl number and a constant Schmidt number specific for each species. The premixed turbulent flames are modeled via the dynamic Thickened Flame (TF) model approach [26]. Unresolved flame wrinkling effects are accounted for using an efficiency function based on the wrinkling factor of Ref. [27]. Flame thickening is not triggered in the discharge region up to the outlet of the SB so that it does not influence the ignition induced by the NRPDs. To ensure a correct resolution of the physical phenomena related to the NRPDs, a very fine mesh is used between the discharge zone and the outlet of the SB. This approach has already proved to be able to account for plasma physics in the same combustor [9, 12]. A complete description of the LES governing equations combined with the dynamic TF model and integrating the phenomenological NEP model is given in Refs [10, 12]. Since plasma chemistry is much faster than flow mixing, its subgrid-scale interaction with turbulence is neglected [11].

The entire combustor geometry represented in Fig. 1 is simulated, including the upstream and downstrem plenums, so that the LES code exhibits self-excited thermoacoustic modes, as in the experiments. The domain is discretized using 74 million tetrahedral elements, body fitted to the combustor geometry. The characteristic cell size is 550 μm in the first and second stage CCs and 800 μm in the dilution air mixer and SB. The grid is further refined to 350 μm in the injection zone for dilution air and fuel, to 130 μm in the discharge region and to 220 μm in the SB after the electrodes where autoignition and/or plasma assisted ignition may occur. The planar cut of the mesh shown in Fig. 1 illustrates the refinement specific to the plasma discharge zone.

4. Results and discussion

4.1. Effects of NRPDs

The LES setup faithfully reproduces the self-excited TI observed in the experiment when NRPD is off (Fig. 3). The fundamental frequency of the TI determined by the LES at $f_{\mathrm{LES}} = 324$ Hz closely aligns with the experimental one $f_{\mathrm{exp.}} = 308$ Hz. The phase shift between the acoustic pressure signal in the first and second stage is about 180° in both the experiment and the LES. Applying NRPDs with the parameters described in Section 2 results in a significant reduction in the TI (Fig. 2). This is retrieved by the LES in which, after 3 to 4 periods, fluctuations in pressure P' and volume-averaged heat release Q' are strongly attenuated (Fig. 3 and animation in the supplementary materials).

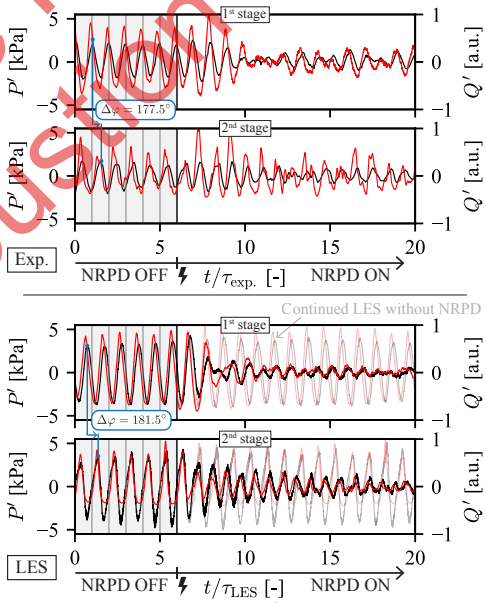

Fig. 3: Fluctuations in pressure P' (black lines) and volume-averaged heat release Q' (red lines) in the first and second stages for both experiments (top) and LES (bottom). The time abscissa is normalized by the period of the instability $\tau_{\mathrm{exp.}} = 1/f_{\mathrm{exp.}}$ and $\tau_{\mathrm{LES}} = 1/f_{\mathrm{LES}}$ with $f_{\mathrm{exp.}} = 308$ Hz and $f_{\mathrm{LES}} = 324$ Hz. NRPDs are applied from $t/\tau = 6$. P' and Q' from a continued LES without NRPD are added to highlight the effect of the NRPDs.

The dynamics of the first and second stage flames are well captured by the LES. This is illustrated in Fig. 4 by comparing the Line-of-Sight (LOS) average

of the HRR for the LES with the OH^* chemiluminescence for the experiments (camera gate 40 μs). The variations in both HRR intensity and flame position are significant for the case "NRPD OFF". The combustion inside the sequential combustor experiences a pronounced oscillation, with the flames contracting periodically before expanding along the CCs and then contracting again. The snapshots in Fig. 4 show a full cycle. For "NRPD ON", the variations in HRR intensity and flame position are small and no longer coherent.

LES data can now be analyzed to study the distribution of acoustic energy production both when the combustor is unstable and during the stabilization induced by the NRPDs. In a low Mach number flow, neglecting viscous terms and variations in molecular weights, a balance equation for the acoustic energy density e_1 can be written using the linearized equations for pressure and velocity perturbations as [28]

$$\frac{\partial e_1}{\partial t} + \nabla \cdot f_1 = r_1 \,, \tag{2}$$

with

$$r_1 = \frac{(\gamma - 1)}{\gamma p_0} p_1 \dot{\omega}_T^1 \text{ and } f_1 = p_1 \boldsymbol{u}_1 \,, \tag{3}$$

where the heat capacity ratio γ and the mean pressure p_0 are constant. p_1, $\dot{\omega}_T^1$ and $\boldsymbol{u}_1$ are the perturbations of pressure, chemical heat release and velocity, respectively. The r_1 term on the right-hand side of Eq. (2) expresses the correlation between unsteady pressure p_1 and heat release $\dot{\omega}_T^1$ and depends on space and time. When the pressure oscillations are in phase with the unsteady heat release, r_1 is positive and locally, there is a production of acoustic energy. Some regions may promote the oscillations by burning more or less in phase with pressure, while other regions may mitigate the oscillations by burning out of phase with pressure. To study the spatial distribution of r_1, an integration over the transverse dimension of the CCs is performed:

$$R_1^z(z,t) = \iiint_{z-\Delta_z}^{z+\Delta_z} r_1(x,y,z^*,t) dx dy dz^* \,, \tag{4}$$

with $\Delta_z = 1.5$ mm. The R_1^z term is distributed along the CCs (Fig. 5). Its value is globally positive, driving the instability, even though it takes negative values for limited times. When the NRPDs are activated, a zone of negative source term rapidly develops in the SB ($z < 125$ mm). In this zone, HRR fluctuations are out of phase with pressure oscillations and provide damping of the acoustic energy. This brings the whole system to a new state where the balance between acoustic energy production and acoustic energy losses is no longer favorable to the development of the TI and thermoacoustic limit cycles. The magnitude of the source term for acoustic energy approaches zero in the first CC, and remains relatively low in the second CC. The integral of the mapped R_1^z term in time and space yields the famous Rayleight integral. Even in the absence of any TI in the combustor, this integral is necessarily positive in a statistically steady state to compensate for losses at the boundaries [28, 29]. The analysis of the acoustic energy budget highlights the role of HRR in the SB to locally act as a sink in presence of NRPDs, reducing the overall acoustic energy production. The chemical activity in the SB is due to plama-induced reactive kernels formation and advection (Fig. 4). This phenomena has already been described by LES and Direct Numerical Simulation (DNS) in Refs [9, 12]. It has been shown that these ignition kernels, initiated after the discharges, provide burning pockets to the sequential flame. However, the characterisation of these plasma-induced kernels has never been done experimentally. In this work, OH-PLIF identifies these advected reactive kernels whose morphology is analogous to that observed numerically (Fig. 6). The flame topology interacting with the kernels is also very similar. This reinforces our conclusions about the capability of the numerical LES setup to accurately reproduce the plasma effects on the main flame.

4.2. Thermoacoustic instability onset

The onset of the TI and the transition to the limit cycle are now analyzed starting from the stable state enabled by the NRPDs. In agreement with the experiments, the TI naturally develops once the NRPDs are deactivated (Fig. 7). Pressure fluctuations in the two CCs exhibit an exponential growth followed by an overshoot before reaching the limit cycle where acoustic energy production and losses are balanced.

Here again, LES data can be used to characterize the acoustic energy production in both stages (Fig. 8). In order to quantify the contribution of each stage to the production of acoustic energy, the source term r_1 (Eq. (3)) is integrated within the i^{th} CC volume V_i:

$$R_1^i(t) = \iiint_{V_i} r_1(x,y,z,t) dV \text{ for } i = 1,2 \,. \tag{5}$$

The R_1^i terms naturally oscillate at twice the TI frequency, with periodic maxima at the TI frequency when both pressure and HRR fluctuations are positive. Averaging R_1^i over a few oscillation periods provides information on the growth of the instability:

$$R_1^{\tau,i}(t) = \frac{1}{2\tau} \int_{t-\tau}^{t+\tau} R_1^i(t) dt \text{ for } i = 1,2 \,, \tag{6}$$

with $\tau = \tau_{\text{LES}} = 1/f_{\text{LES}}$. The $R_1^{\tau,i}$ terms grow as the TI develops, before reaching a steady state at the limit cycle (Fig. 8). An overshoot period is visible on the $R_1^{\tau,1}$ term that may be responsible for the overshoot in pressure fluctuations (Fig. 7). During the growth of the instability, the overshoot period and the limit cycle, $R_1^{\tau,2}$ is about five times greater than $R_1^{\tau,1}$. Therefore, despite the two stages featuring similar thermal power, the acoustic energy production in

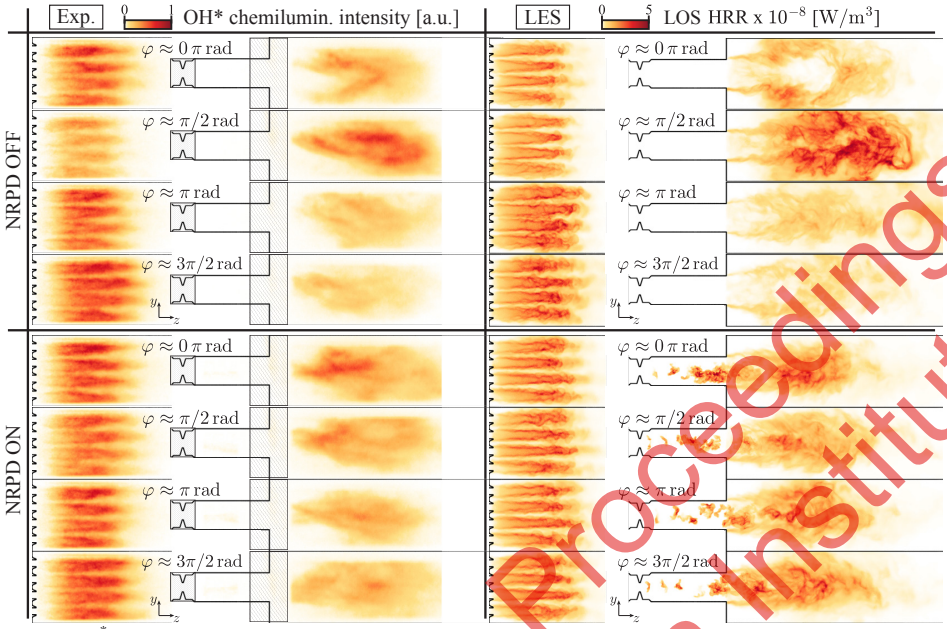

Fig. 4: Left: OH* chemiluminescence images in the first and second stages (camera gate 40 μs, recorded from the x-direction). Right: LOS averaged HRR along the x-axis from LES snapshots. Four different instants in the thermoacoustic cycle are shown when NRPDs are off (top) and on (bottom). The phase φ is given with an accuracy of ± 0.2 rad.

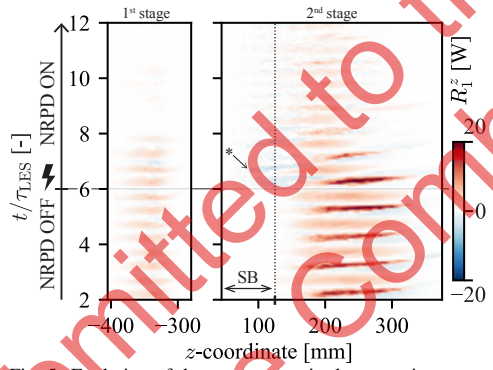

Fig. 5: Evolution of the source term in the acoustic energy balance equation (Eq. (2)) when NRPDs are turned on: Distribution of the axial acoustic energy source term $R_1^z(z,t)$ (Eq. (4)) in the first stage CC (left) and in the second stage CC (right). The negative R_1^z values in the SB when NRPDs are turned on are highlighted by an arrow preceded by '$*$'.

the second CC significantly contributes to the overall acoustic energy budget, playing a crucial role in the development of the self-excited TI. This could explain why, in addition to being placed in a favorable environment (i.e., hot reactive mixture), NRPDs applied in the SB are so effective [7].

5. Conclusion

Numerical simulation of the stabilization of a thermoacoustically unstable combustor using NRPDs is successfully performed for the first time. This has been achieved through the use of a massively parallel LES solver combined with a precise description of the chemical kinetics and a state-of-the-art model for the plasma effects, together with an experimental platform for validation.

The plasma-induced reactive kernels initiated in the SB of the sequential combustor that are observed in the present simulation and in Refs [9, 12] are characterized experimentally using OH-PLIF. An analysis of the source term in the acoustic energy balance equation reveals that these kernels generate heat release fluctuations that are in phase opposition to those associated with the acoustic pressure in the SB. It induces locally a sink term in the acoustic energy balance equation that reduces the overall acoustic energy production in the second stage. The combustor then reaches a new state of equilibrium where it is no longer thermoacoustically unstable.

In addition, the evolution of the acoustic energy source term is studied during the onset of the TI. The magnitude of the source term is about five times greater in the second stage than in the first, both during the growth and the limit cycle. This demonstrates that the second stage plays a major role in the TI observed for the conditions of operation considered in this study.

This work not only sheds light on plasma thermoacoustic stabilization mechanisms, but also provides a

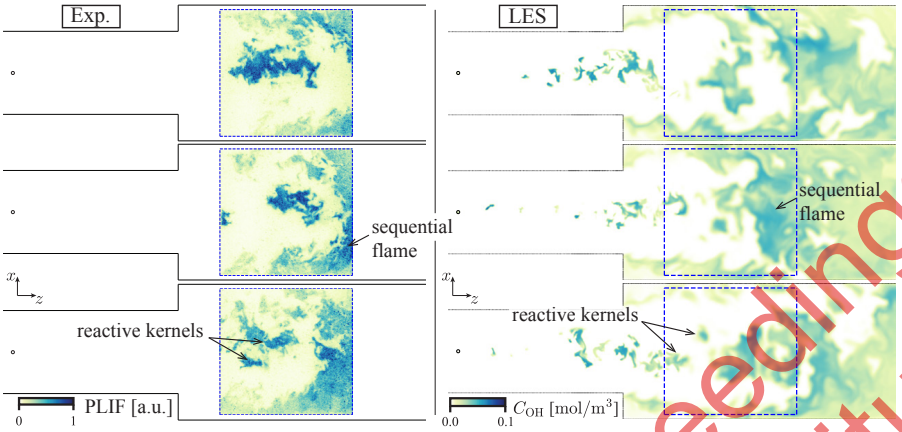

Fig. 6: Left: OH-PLIF snapshots of the reactive kernels initiated by the NRPDs in the SB and feeding the sequential flame. Right: Planar cut of LES snapshots colored by the OH concentration C_{OH} retrieving the convection of reactive kernels through the SB.

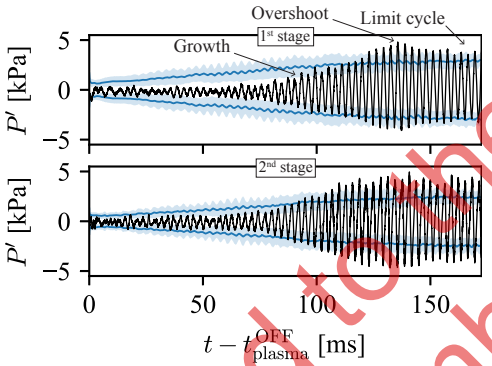

Fig. 7: Evolution of the pressure fluctuations after plasma is turned off due to the self-excited TI in the LES. The mean experimental envelope of the pressure fluctuations is added using blue solid lines. The standard deviation is indicated by the filled blue areas. Statistics have been computed using 40 experimental realisations.

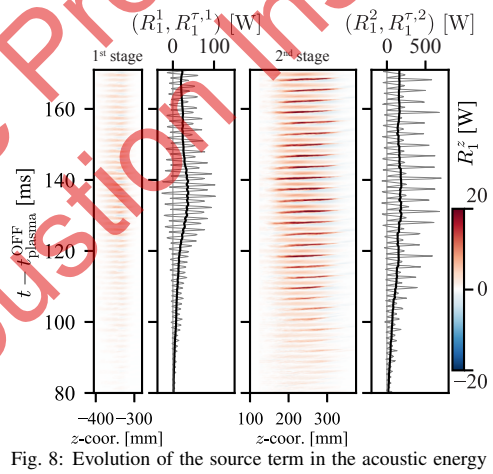

Fig. 8: Evolution of the source term in the acoustic energy balance equation (Eq. (2)) when the TI sets in: Distribution of the axial acoustic energy source term $R_1^z(z,t)$ (Eq. (4), color plot); Evolution of the volume integrated acoustic energy source term $R_1^i(t)$ (Eq. (5), thin lines) and the volume integrated and phase averaged acoustic energy source term $R_1^{\tau,i}(t)$ (Eq. (6), thick lines). Values are given both in the first stage CC (left) and in the second stage CC (right).

robust simulation framework for the study of the stabilization of TIs using NRPDs in a sequential combustor, paving the way for studies in other configurations and/or other operating conditions. This is the case, for example, of another study conducted by the authors concurrently with the present work [30], where the effects of ultra-low power plasma [7] on the second stage of a sequential combustor are studied. The study uses special forced flow simulations that cannot be achieved experimentally, but that are crucial for predicting the acoustic amplification potential of the sequential stage at a given condition.

Declaration of competing interest

The authors declare that they have no known competing financial interests or personal relationships that could have appeared to influence the work reported in this paper.

Acknowledgments

This project has received funding from the European Research Council (ERC) under the European Union's Horizon 2020 research and innovation programme (grant agreement No [820091]). This work was supported by a grant from the Swiss National Supercomputing Centre (CSCS) under project ID s1220.

The authors gratefully acknowledge CERFACS for providing the LES solver AVBP and the antares and ARCANE libraries.

Supplementary materials

Supplementary materials associated with this article can be found, in the online version, at doi:xxx.

References

[1] D. A. Lacoste, Flames with plasmas, Proc. Combust. Inst. 39 (4) (2022) 5405–5428.

[2] D. A. Lacoste, J. P. Moeck, D. Durox, C. O. Laux, T. Schuller, Effect of nanosecond repetitively pulsed discharges on the dynamics of a swirl-stabilized lean premixed flame, J. Eng. Gas Turbines Power 135 (10) (2013) 101501.

[3] W. Kim, J. Snyder, J. Cohen, Plasma assisted combustor dynamics control, Proc. Combust. Inst. 35 (3) (2015) 3479–3486.

[4] J. M. Bonebrake, D. L. Blunck, J. K. Lefkowitz, T. M. Ombrello, The effect of nanosecond pulsed high frequency discharges on the temperature evolution of ignition kernels, Proc. Combust. Inst. 37 (4) (2019) 5561–5568.

[5] A. M. Alkhalifa, A. Alsalem, D. Del Cont-Bernard, D. A. Lacoste, Active control of thermoacoustic fluctuations by nanosecond repetitively pulsed glow discharges, Proc. Combust. Inst. 39 (4) (2023) 5429–5437.

[6] L. Yu, B. Aravind, D. A. Lacoste, Mitigating the response of premixed swirl flames to acoustic excitation by nanosecond repetitively pulsed discharges at elevated pressures, Combust. Flame 256 (2023) 112944.

[7] B. Dharmaputra, S. Shcherbanev, B. Schuermans, N. Noiray, Thermoacoustic stabilization of a sequential combustor with ultra-low-power nanosecond repetitively pulsed discharges, Combust. Flame 258 (2023) 113101.

[8] Y. Bechane, B. Fiorina, Numerical analysis of turbulent flame enhancement by nanosecond repetitively pulsed plasma discharges, Proc. Combust. Inst. 39 (4) (2022) 5465–5476.

[9] Q. Malé, S. Shcherbanev, N. Noiray, Numerical study of plasma assisted combustion in a sequential combustor, Proc. Combust. Inst. 39 (4) (2022) 5447–5456.

[10] N. Barléon, B. Cuenot, O. Vermorel, Large-Eddy Simulation of swirled flame stabilisation using NRP discharges at atmospheric pressure, Appl. Energy Combust. Sci. 15 (February) (2023) 100163.

[11] Y. Bechane, B. Fiorina, Numerical investigations of turbulent premixed flame ignition by a series of Nanosecond Repetitively Pulsed discharges, Proc. Combust. Inst. 38 (4) (2021) 6575–6582.

[12] Q. Malé, N. Barléon, S. Shcherbanev, B. Dharmaputra, N. Noiray, Numerical study of nitrogen oxides chemistry during plasma assisted combustion in a sequential combustor, Combust. Flame 260 (2024) 113206.

[13] N. Barléon, L. Cheng, B. Cuenot, O. Vermorel, A phenomenological model for plasma-assisted combustion with NRP discharges in methane-air mixtures: PACMIND, Combust. Flame 253 (2023) 112794.

[14] S. Yang, S. Nagaraja, W. Sun, V. Yang, Multi-scale modeling and general theory of non-equilibrium plasma-assisted ignition and combustion, J. Phys. D. Appl. Phys. 50 (43) (2017) 433001.

[15] A. Bellemans, N. Kincaid, N. Deak, P. Pepiot, F. Bisetti, P-DrGEP: A novel methodology for the reduction of kinetics mechanisms for plasma-assisted combustion applications, Proc. Combust. Inst. 38 (4) (2021) 6631–6639.

[16] A. Duarte Gomez, N. Deak, F. Bisetti, Jacobian-free newton–krylov method for the simulation of non-thermal plasma discharges with high-order time integration and physics-based preconditioning, J. Comput. Phys. 480 (2023) 112007.

[17] M. Castela, B. Fiorina, A. Coussement, O. Gicquel, N. Darabiha, C. O. Laux, Modelling the impact of non-equilibrium discharges on reactive mixtures for simulations of plasma-assisted ignition in turbulent flows, Combust. Flame 166 (2016) 133–147.

[18] L. Cheng, N. Barleon, B. Cuenot, O. Vermorel, A. Bourdon, Plasma assisted combustion of methane-air mixtures: Validation and reduction, Combust. Flame 240 (2022) 111990.

[19] T. Schönfeld, M. Rudgyard, Steady and unsteady flow simulations using the hybrid flow solver AVBP, AIAA J. 37 (11) (1999) 1378–1385.

[20] L. Y. Gicquel, N. Gourdain, J. F. Boussuge, H. Deniau, G. Staffelbach, P. Wolf, T. Poinsot, Calcul parallèle haute performance des écoulements en géométries complexes, Comptes Rendus - Mec. 339 (2-3) (2011) 104–124.

[21] O. Colin, M. Rudgyard, Development of High-Order Taylor-Galerkin Schemes for LES, J. Comput. Phys. 162 (2) (2000) 338–371.

[22] F. Nicoud, H. B. Toda, O. Cabrit, S. Bose, J. Lee, Using singular values to build a subgrid-scale model for large eddy simulations, Phys. Fluids 23 (8) (2011) 085106.

[23] T. J. Poinsot, S. K. Lelef, Boundary conditions for direct simulations of compressible viscous flows, J. Comput. Phys. 101 (1) (1992) 104–129.

[24] P. Schmitt, T. Poinsot, B. Schuermans, K. P. Geigle, Large-eddy simulation and experimental study of heat transfer, nitric oxide emissions and combustion instability in a swirled turbulent high-pressure burner, J. Fluid Mech. 570 (2007) 17–46.

[25] G. Bagheri, E. Ranzi, M. Pelucchi, A. Parente, A. Frassoldati, T. Faravelli, Comprehensive kinetic study of combustion technologies for low environmental impact: MILD and OXY-fuel combustion of methane, Combust. Flame 212 (2020) 142–155.

[26] J. P. Legier, T. Poinsot, D. Veynante, Dynamically thickened flame LES model for premixed and non-premixed turbulent combustion, Proc. Summer Program, Cent. Turbul. Res. (2000) 157–168.

[27] F. Charlette, C. Meneveau, D. Veynante, A power-law flame wrinkling model for LES of premixed turbulent combustion Part I: Non-dynamic formulation and initial tests, Combust. Flame 131 (1-2) (2002) 159–180.

[28] T. Poinsot, D. Veynante, Theoretical and Numerical Combustion, 2022.

[29] B. Schuermans, J. Moeck, A. Blondé, B. Dharmaputra, N. Noiray, The Rayleigh integral is always positive in steadily operated combustors, Proc. Combust. Inst. 39 (4) (2023) 4661–4669.

[30] M. Impagnatiello, Q. Malé, N. Noiray, Acoustic scattering of a sequential combustor controlled with non-equilibrium plasma: a numerical study, Submitted to the CI's 40th Int. Symposium (2023).